Spatial distributions of elastically backscattered electrons from copper and silver

1999 J. Phys. D: Appl. Phys. 32 3122

(http://iopscience.iop.org/0022-3727/32/24/305)

J. Phys. D: Appl. Phys. **32** (1999) 3122–3127. Printed in the UK PII: S0022-3727(99)06322-6

Spatial distributions of elastically backscattered electrons from copper and silver

C M Kwei†, C J Hung†, P Su† and C J Tung‡

† Department of Electronics Engineering, National Chiao Tung University, Hsinchu 300, Taiwan
‡ Department of Nuclear Science, National Tsing Hua University, Hsinchu 300, Taiwan

E-mail: cmkwei@cc.nctu.edu.tw

Received 26 July 1999

Abstract. We investigated the spatial distributions regarding the pathlength, the penetration depth, and the lateral displacement of 200–2000 eV electrons elastically backscattered from copper and silver. We calculated these distributions by the Monte Carlo method using elastic scattering cross sections and inelastic inverse mean free paths for volume and surface excitations. In our approach, we applied the partial wave expansion method and the finite difference technique to calculate electron elastic cross sections by the Hartree–Fock–Winger–Seitz scattering potential for solid atoms. We employed the extended Drude dielectric function to estimate electron inelastic mean free paths inside the solid and electron surface excitation parameters outside the solid. Our study was focused on the energy dependence of the pathlength distribution, the maximum depth distribution and the radial distribution. We found that both the radial displacement and the maximum depth of backscattered electrons were on the order of a few angstroms. The maximum depth and the pathlength distributions obeyed the exponential attenuation form. The ratio of the attenuation lengths for the pathlength and the maximum depth distributions saturated to a value somewhat greater than two. Considering the back and forth trajectories of backscattered electrons, it revealed that most electrons were backscattered from the solid through a single elastic scattering or a few elastic scatterings. As electron energy decreases, this ratio became larger, indicating that the probability for smaller scattering angles increases.

1. Introduction

The elastic backscattering of electrons from solid surfaces plays an important role in many applications [1–7] such as elastic peak electron spectroscopy (EPES), Auger electron spectroscopy (AES), scanning electron microscopy (SEM), reflection electron energy loss spectroscopy (REELS) and disappearance potential spectroscopy (DAPS), etc. In the case of EPES, for instance, the intensity and angular distributions of elastically backscattered electrons contain information on electron elastic and inelastic interactions with the solids. These distributions are usually characterized by the elastic reflection coefficient and the angular distribution function. Theories are available for the calculation of these quantities by using the Monte Carlo method [8–12] or the Boltzmann transport equation [13–15].

In this paper, we investigated the spatial distributions in the pathlength, the maximum penetration depth and the radial or lateral displacement of electrons elastically backscattered from Cu and Ag. These distributions are important for quantitative analyses of surface spectroscopic data. For example, one may extract electron inelastic cross sections from REELS data using the pathlength distribution function [16, 17]. Calculations of this function are available by the solution of the transport equation in different approximations [13, 18–20]. In the so-called P_1-approximation, neither the elastic differential cross section nor the surface boundary condition was explicitly employed. In the transport approximation, however, the elastic differential cross section was replaced by the isotropic transport cross section. Since elastic interactions cause angular deflections that alter electron pathlengths, the spatial distributions of elastically backscattered electrons strongly depend on the differential elastic scattering cross sections. Hence, in this work we calculated the spatial distributions by the Monte Carlo method, based on detailed elastic scattering cross sections and inelastic mean free paths for volume and surface excitations. In our approach, we applied the partial wave expansion method [12] and the finite difference technique [9] to calculate electron elastic scattering cross sections using a Hartree–Fock–Winger–Seitz, solid-atom potential [21]. The dielectric response function [22] was employed to estimate electron inelastic mean free paths inside the solid and surface excitation parameters [23, 24] near the surface. Our study was focused on the energy dependence of the pathlength distribution, the maximum depth distribution and the radial distribution of electrons elastically backscattered from Cu and Ag. We found that

0022-3727/99/243122+06$30.00

most electrons were backscattered from the solid through a single elastic scattering or a few elastic scatterings. The radial displacement of backscattered electrons from their impinging point on the surface was quite short, on the order of a few angstroms. Both the maximum depth and the pathlength distributions obeyed the exponential attenuation form. For an electron of energy greater than 500 eV in Ag, the attenuation length for pathlength distribution was about 2.4 times the attenuation length for maximum depth distribution. As the electron energy decreases, the ratio of the attenuation lengths between these two distributions became larger, indicating that the probability for smaller scattering angles was increasing.

2. Theory

2.1. Stochastic interaction processes

Electrons impinging on a solid cause elastic and inelastic interactions as they travel across the surface and inside the solid. Elastic scatterings lead to angular deflections that alter the directions of electron movements. Inelastic interactions, on the other hand, are responsible for the energy lost by electrons. Monte Carlo simulations of elastically backscattered electrons trace electrons from their impinging point on the surface to the emerging point by recording electron trajectories. Each trajectory consists of a linear pathlength between two successive elastic scatterings. An inelastic interaction causing energy loss makes no contribution to the elastically backscattered electrons. Since the occurrence of elastic scatterings obeys the Poisson stochastic process, the probability distribution function of a pathlength, s, follows the exponential form [25]

$$P(s) = \frac{1}{\lambda_e} \exp\left(-\frac{s}{\lambda_e}\right). \tag{1}$$

Here the elastic mean free path of electrons is determined by

$$\lambda_e = (N\sigma_e)^{-1} \tag{2}$$

where N is the atomic density of the solid. The total elastic cross section is calculated by

$$\sigma_e = \int \frac{\mathrm{d}\sigma_e}{\mathrm{d}\Omega}\,\mathrm{d}\Omega \tag{3}$$

where $\mathrm{d}\sigma_e/\mathrm{d}\Omega$ is the differential elastic cross section and $\mathrm{d}\Omega = \sin\theta\,\mathrm{d}\theta\,\mathrm{d}\phi$ is the differential solid scattering angle. Due to the cylindrical symmetry of the scattering, the elastic scattering follows a uniform distribution about the azimuthal angle, ϕ. The polar angle, θ, is determined by the probability density function as

$$P(\theta) = \frac{2\pi \sin\theta}{\sigma_e}\frac{\mathrm{d}\sigma_e}{\mathrm{d}\Omega}. \tag{4}$$

The tracking of electrons continues until either they leave the solid or their trajectory paths become so large that the contribution to the elastically backscattered intensity can be neglected. The contribution to the elastically backscattered intensity from the jth electron trajectory is given by

$$\Delta I_j = \begin{cases} \mathrm{e}^{-P_s(\alpha_{Ij})}\,\mathrm{e}^{-P_s(\alpha_{Rj})}\,\mathrm{e}^{-s_j/\lambda_i} \\ \qquad \text{for backscattered electrons within} \\ \qquad \text{pre-selected acceptance angles} \\ 0 \qquad \text{otherwise} \end{cases} \tag{5}$$

where s_j is the pathlength of the jth electron trajectory, P_s is the probability of surface excitations as the electron crosses the vacuum–solid interface, λ_i is the electron inelastic mean free path, and α_{Ij} and α_{Rj} are, respectively, the incident and reflected angles between the electron velocity and the surface normal for incident and backscattered electrons. The factors $\exp[-P_s(\alpha_{Ij})]$ and $\exp[-P_s(\alpha_{Rj})]$ are the probabilities that incident and backscattered electrons travel across the surface without surface excitations, respectively. The factor $\exp(-s_j/\lambda_i)$ is the probability that the electron travels a pathlength s_j inside the solid without inelastic interactions.

2.2. Elastic and inelastic differential cross sections

The accuracy of Monte Carlo simulations depends on the differential interaction cross sections. The input data in the Monte Carlo simulations include differential elastic cross sections, inelastic inverse mean free paths and surface excitation probabilities. Previously we have developed models [9–11, 23, 24] for the calculations of these quantities. The differential elastic cross section is given in the partial wave expansion method as

$$\frac{\mathrm{d}\sigma_e}{\mathrm{d}\Omega} = \frac{1}{8\pi}\left|\sum_{\ell=0}^{\infty}(2\ell+1)(\mathrm{e}^{2\mathrm{i}\delta_\ell}-1)P_\ell(\cos\theta)\right|^2 \tag{6}$$

where δ_ℓ is the phase shift of the ℓth partial wave, P_ℓ is the Lengendre polynomial of degree ℓ and ℓ is the orbital angular momentum quantum number. For the determination of phase shifts, the finite difference technique is applied in the solution of the radial Schrödinger equation. Here the Hartree–Fock–Wigner–Seitz scattering potential for solid atoms is employed.

Considering a semi-infinite solid at $z < 0$, the differential inelastic inverse mean free path depends on whether the electron is moving from vacuum to solid, $v \to s$, or from solid to vacuum, $s \to v$. For normally incident and escaping electrons of velocity v and energy $E = v^2/2$, the differential inelastic inverse mean free paths $\mu_i^{s\to v}(E,\omega,z)$ and $\mu_i^{v\to s}(E,\omega,z)$ are given by [23, 24]

$$\begin{aligned}\mu_i^{s\to v}(E,\omega,z) = {} & \frac{1}{\pi^2 v}\int \mathrm{d}^2Q\frac{v}{\omega^2+(vQ)^2} \\ & \times\left\{2\,\mathrm{Im}\left(\frac{-1}{\varepsilon+1}\right)\mathrm{e}^{-Q|z|}\left[2\cos\left(\frac{\omega z}{v}\right)-\mathrm{e}^{-Q|z|}\right]\Theta(z)\right. \\ & +\left[2\,\mathrm{Im}\left(\frac{-1}{\varepsilon+1}\right)\mathrm{e}^{-2Q|z|}+\mathrm{Im}\left(\frac{-1}{\varepsilon}\right)(1-\mathrm{e}^{-2Q|z|})\right] \\ & \left.\times\Theta(-z)\right\}\end{aligned} \tag{7}$$

and

$$\begin{aligned}\mu_i^{v\to s}(E,\omega,z) = {} & \frac{1}{\pi^2 v}\int \mathrm{d}^2Q\frac{v}{\omega^2+(vQ)^2} \\ & \times\left\{2\,\mathrm{Im}\left(\frac{-1}{\varepsilon+1}\right)\mathrm{e}^{-2Q|z|}\Theta(z)+\left\{2\,\mathrm{Im}\left(\frac{-1}{\varepsilon+1}\right)\mathrm{e}^{-Q|z|}\right.\right. \\ & \times\left[2\cos\left(\frac{\omega z}{v}\right)-\mathrm{e}^{-Q|z|}\right]+\mathrm{Im}\left(\frac{-1}{\varepsilon}\right) \\ & \left.\left.\times\left[1+\mathrm{e}^{-2Q|z|}-2\mathrm{e}^{-Q|z|}\cos\left(\frac{\omega z}{v}\right)\right]\right\}\Theta(-z)\right\}\end{aligned} \tag{8}$$

where Θ is the step function, ω is the energy transfer, $\vec{q} = (\vec{Q}, q_z)$ is the momentum transfer, the upper and lower limits of integration are $Q_+ = [q_+^2 - (\omega/v)^2]^{1/2}$ and $Q_- = [q_-^2 - (\omega/v)^2]^{1/2}$ and $q_\pm = \sqrt{2E} \pm \sqrt{2(E-\omega)}$. Note that those terms involving $\mathrm{Im}[-1/(\varepsilon+1)]$ are the contributions from surface excitations; whereas those containing $\mathrm{Im}(-1/\varepsilon)$ are from volume excitations.

The corresponding inelastic inverse mean free paths of electrons are given by

$$\mu_i^{s\to v}(E,z) = \int_0^E \mu_i^{s\to v}(E,\omega,z)\,\mathrm{d}\omega \tag{9}$$

and

$$\mu_i^{v\to s}(E,z) = \int_0^E \mu_i^{v\to s}(E,\omega,z)\,\mathrm{d}\omega. \tag{10}$$

Equations (9) and (10) indicate that the inelastic inverse mean free path depends on the depth, z, of electron inside the solid. When an electron travels near the surface inside the solid, surface excitations dominate the contribution to the inelastic inverse mean free path. On the other hand, volume excitations dominate this contribution as an electron moves deep inside the solid. The total, surface and volume, inelastic inverse mean free paths are, however, roughly depth independent due to the approximate compensation of volume and surface excitations. As an electron travels outside the solid, but near the surface, the inelastic inverse mean free path is completely contributed to by surface excitations. To characterize the probability of surface excitations outside the solid, it is general to use the surface excitation parameter defined by [24]

$$P_s^{s\to v}(E) = \int_0^\infty \mathrm{d}z \int_0^E \mu^{s\to v}(E,\omega,z)\,\mathrm{d}\omega \tag{11}$$

for an electron moving from solid to vacuum and

$$P_s^{v\to s}(E) = \int_0^\infty \mathrm{d}z \int_0^E \mu^{v\to s}(E,\omega,z)\,\mathrm{d}\omega \tag{12}$$

for electron moving from vacuum to solid. Note that the dependence of the surface excitation parameter on the incident and escaping electrons follows the approximate relations

$$P_s^{s\to v}(E) \text{ or } P_s^{v\to s}(E) = aE^{-b} \tag{13}$$

where a and b are fitting parameters. For the surface excitation parameters of obliquely incident and escaping electrons, one may multiply the surface excitation parameters of normally incident and escaping electrons by $(\cos\alpha)^{-1}$, where α is the angle between the electron velocity and the surface normal.

3. Results and discussion

The Monte Carlo algorithm described above was applied for the simulation of electrons with energies between 200 and 2000 eV elastically backscattered from Cu and Ag. Figure 1 illustrates this simulation by showing the total pathlength R, the maximum depth z and the radial displacement r of simulated electrons. The total pathlength is the sum of all of the individual pathlengths inside the solid, i.e. $R = R_1 + R_2 + R_3 + \cdots$. Figure 2 shows the differential elastic

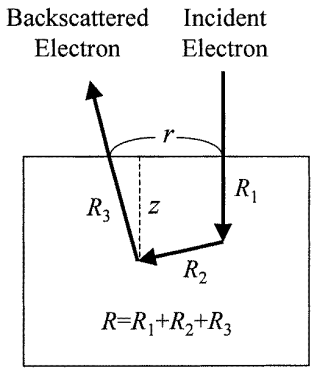

Figure 1. A schematic diagram for electrons elastically backscattered from solid surfaces. The radial displacement, r, the maximum depth, z, and the total pathlength, $R = R_1 + R_2 + R_3$, are displayed.

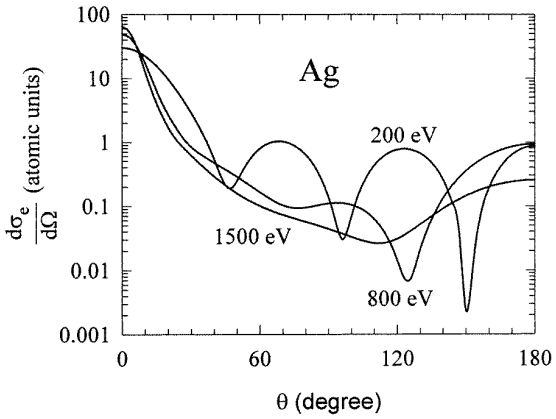

Figure 2. A plot of the differential elastic cross sections (in atomic units) as a function of the scattering angle for electrons of various energies in Ag. The elastic scattering potential was derived from a Hartree–Fock–Wigner–Seitz electron density distribution [21] for solid atoms.

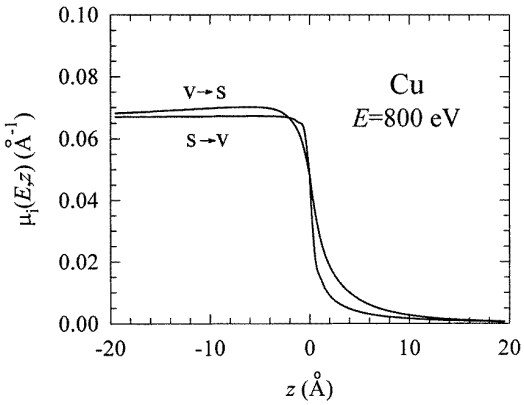

Figure 3. A plot of the inelastic inverse mean free paths for an 800 eV electron normally incident into (vacuum to solid) and escaping from (solid to vacuum) Cu. The inelastic inverse mean free path extends to more than 10 Å outside the solid ($z > 0$) due to surface excitations. Both surface and volume excitations contribute to the inelastic inverse mean free path inside the solid ($z < 0$).

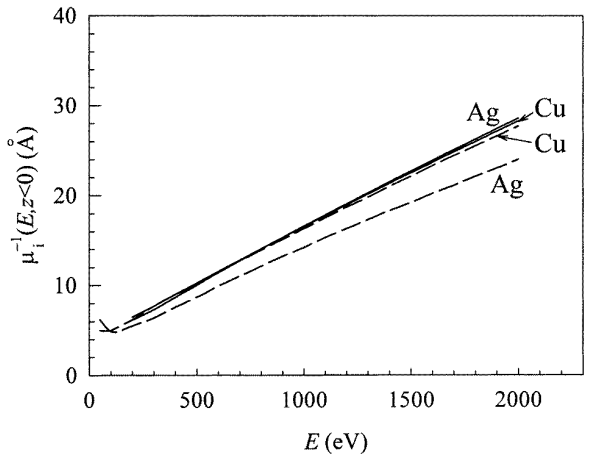

Figure 4. A comparison of the spatially non-varying electron inelastic mean free paths in Cu and Ag as a function of the electron energy calculated in the present work (full curves) and by Tanuma *et al* [26] (broken curves). The calculations of Tanuma *et al* applied the Lindhard dielectric function for free-electron gases. Our calculations made use of a modified Drude dielectric function [22] that allowed band structures of the energy loss function.

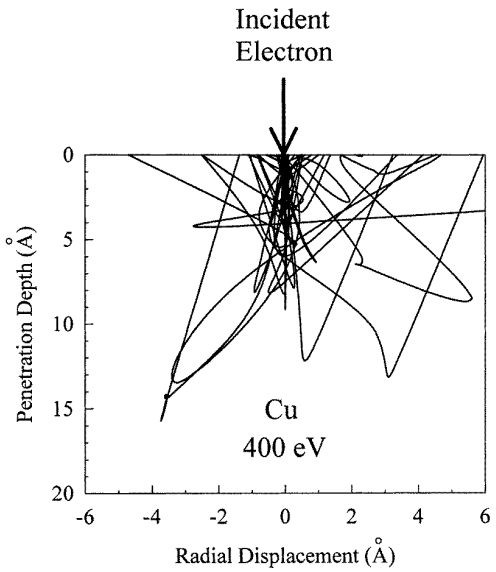

Figure 5. A projection view of the Monte Carlo simulation results for 400 eV electrons elastically backscattered from Cu at normal incidence. The abscissa and ordinate are, respectively, the radial displacement and the penetration depth of the backscattered electrons.

cross sections calculated using the partial wave expansion method and the finite difference technique as a function of scattering angle for electrons of 200, 800 and 1500 eV in Ag. Note that the elastic scattering potential was derived from a Hartree–Fock–Wigner–Seitz electron density distribution. The fluctuation of the curves in this figure is due to the screening of the nuclear charge by shell-wise electrons in the solid atom. Based on the extended Drude-type dielectric function [22], we calculated electron inelastic mean free paths using equations (7)–(10). Figure 3 shows the inelastic inverse mean free path for an 800 eV electron normally incident into or escaping from Cu. It is seen that the inelastic inverse mean free path extends to a region more than 10 Å outside the

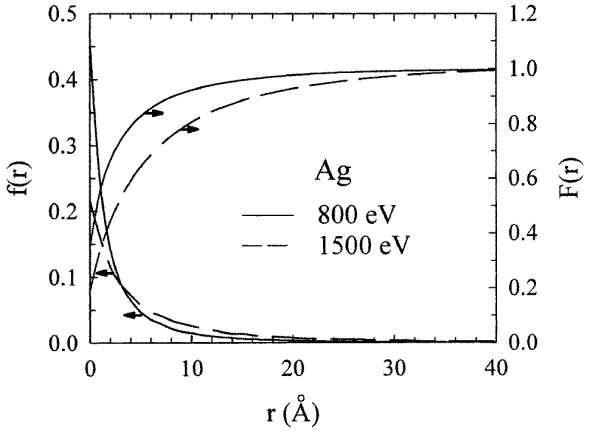

Figure 6. The differential (left ordinate) and the accumulated (right ordinate) distributions for the radial displacement of 800 and 1500 eV electrons elastically backscattered from Ag at normal incidence.

solid due to surface excitations. Inside the solid the surface effect is, however, compensated by volume excitations, in that the inelastic (surface and volume) mean free path quickly saturates within a few angstroms from the surface. Therefore, a spatially non-varying electron inelastic mean free path holds approximately true inside the solid. Figure 4 is a comparison of such a spatially non-varying electron inelastic mean free path in Cu and Ag as a function of the electron energy calculated presently (full curves) and by Tanuma *et al* [26] (broken curves). The calculations of Tanuma *et al* applied the Lindhard dielectric function for free-electron gases with experimental optical data. Our calculations made use of an extended Drude dielectric function that allowed the band structures of the energy loss function. The present results show that electron inelastic mean free path in Ag is a little larger than that in Cu for electron energies greater than 1000 eV. Although this circumstance is consistent with the calculations of the electron gas statistical model [27], it is reversed from those given by Tanuma *et al*. The difference between the results of the present work and Tanuma *et al* for both Cu and Ag is not excessive in view of the uncertainties in the different dielectric functions and optical data used in these two approaches. The surface excitation parameter determined using (11) and (12) was given in Kwei *et al* [24].

The Monte Carlo simulation of elastically backscattered electrons provides the possibility for an insight view of electron trajectories inside the solid. From this view, the radial distance, maximum depth and pathlength distributions can be investigated. Figure 5 is a projection view of Monte Carlo results on the trajectories of 400 eV electrons elastically backscattered from Cu at normal incidence. One sees that most backscattered electrons interact with the solid through a single elastic scattering. The radial distribution functions plotted in figure 6 are for 800 and 1500 eV electrons backscattered from Ag at normal incidence. It shows that most electrons are backscattered from the surface with small radial displacement from the incident beam. It also shows that the distribution at a small radial displacement is enhanced as the electron energy decreases. The accumulated radial distribution function plotted in this figure (using the right-hand side ordinate scale) indicates that nearly 95% of the

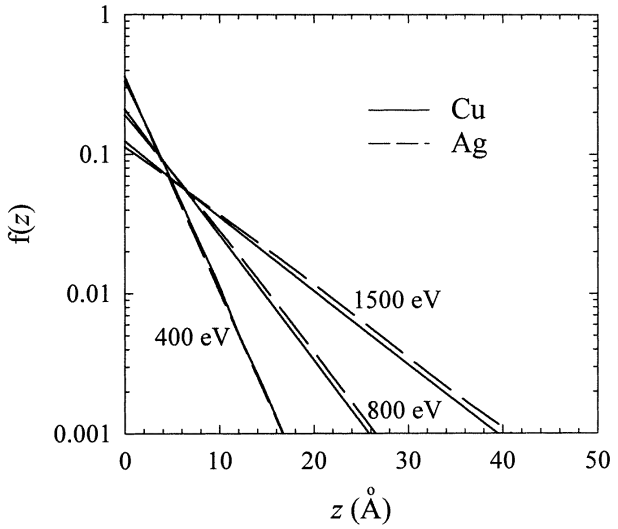

Figure 7. The maximum depth distributions for 400, 800 and 1500 eV electrons elastically backscattered from Cu and Ag at normal incidence. A semi-logarithmic plot is made to indicate the exponential dependence of the distribution on the maximum penetration depth.

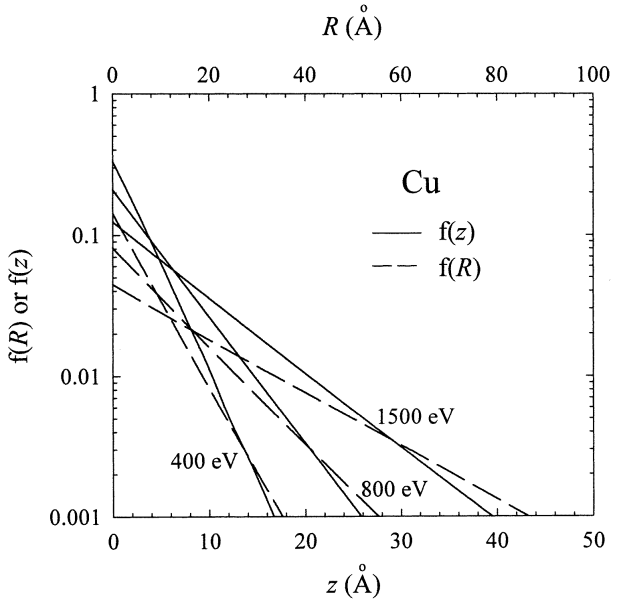

Figure 8. A semi-logarithmic plot of the pathlength (upper abscissa) distributions for 400, 800 and 1500 eV electrons elastically backscattered from Cu at normal incidence. For comparison, corresponding maximum depth (lower abscissa) distributions are also plotted. Note that the scale for the pathlength is twice that for the maximum depth to account for the back and forth trajectories of backscattered electrons.

800 eV electrons are backscattered with radial displacement less than 10 Å.

Figure 7 shows the distribution of the maximum penetration depth for elastically backscattered electrons of 400, 800 and 1500 eV in Cu and Ag at normal incidence. The straight lines in this semi-logarithmic plot reveal that the maximum depth distribution obeys an exponential form, i.e.

$$f(z) \propto \exp(-z/L_D) \tag{14}$$

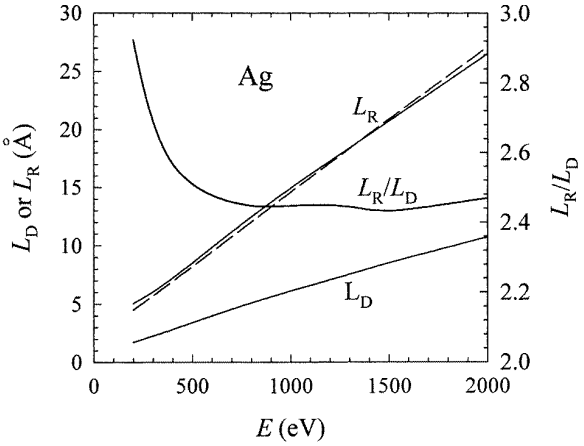

Figure 9. The attenuation length for the pathlength distribution, L_R, the attenuation length for the maximum depth distribution, L_D, and their ratio, L_R/L_D, of electrons elastically backscattered from Ag. The full curves are the results of the present calculations. The broken curve is the attenuation length for the pathlength distribution calculated using (16) of the P_1-approximation.

where L_D is the attenuation length for the maximum depth distribution. Note that this length increases with increasing electron energy.

The pathlength distribution functions calculated for the 400, 800 and 1500 eV electrons elastically backscattered from Cu at normal incidence are plotted in figure 8. It is seen that this function also follows an exponential form, i.e.

$$f(R) \propto \exp(-R/L_R) \tag{15}$$

where L_R is the attenuation length for the pathlength distribution. To explore the relationship between pathlength and maximum depth, we plot in this figure the corresponding maximum depth distribution. Note that the scale for the pathlength (upper abscissa) is twice that for the maximum depth (lower abscissa) to account for the back and forth trajectories of the backscattered electrons. If the electrons were backscattered through a single elastic scattering with 180° scattering angle then $R = 2z$. For a single elastic scattering with other scattering angles then $R > 2z$. For electrons backscattered through multiple elastic scatterings, $R - 2z$ further increases and spreads out. Since the pathlength distribution is a composite distribution in both radial displacement and maximum depth, it is evident from figure 8 that the pathlength distribution is broader than the maximum depth distribution. The pathlength and maximum depth distributions become even broader as the electron energy increases, indicating that multiple scatterings are more probable.

Figure 9 shows a plot of the energy dependence of the attenuation lengths for the pathlength distribution, L_R, and for the maximum depth distribution, L_D, of electrons elastically backscattered from Ag. Both attenuation lengths increase linearly with electron energy. These attenuation lengths can be determined either from the slopes of the straight lines in figure 8 or from Monte Carlo calculations of the mean pathlength or mean maximum depth. We found that the attenuation lengths determined by both methods agree with each other quite well. Also shown in this figure is the

ratio of the attenuation length for the pathlength distribution to that for the maximum depth distribution. This ratio seems relatively energy independent for an electron energy greater than ∼500 eV. As the electron energy decreases, this ratio becomes larger, indicating that the probability for smaller scattering angles is increasing.

Previously, Tofterup [13] made use of the Boltzmann equation and the P_1-approximation to derive the pathlength distribution for electrons in REELS. They found that this distribution was approximately $\propto e^{-R/L}$, where $L \approx 2\lambda_t$ is the characteristic length and λ_t is the transport elastic mean free path. According to the Poisson stochastic process, the pathlength distribution of elastically backscattered electrons is therefore $\propto \exp(-R/\lambda_i)\exp(-R/L)$. Thus the attenuation length for the pathlength distribution is given by

$$L_R = \frac{2\lambda_t\lambda_i}{2\lambda_t + \lambda_i}. \tag{16}$$

As an example, figure 9 shows a comparison of the attenuation length for the pathlength distribution in Ag determined from the slope of this distribution in semi-logarithmic plot (full curves) and calculated from equation (16) (broken curve). Good agreement is observed.

4. Conclusion

In this work, we investigated the spatial distributions for the pathlength, the penetration depth and the radial displacement of electrons with energies between 200 and 2000 eV elastically backscattered from copper and silver. Monte Carlo simulations were performed using electron elastic and inelastic interaction cross sections from model calculations. We found that the radial displacement and the maximum depth of backscattered electrons were of the order of a few angstroms. The maximum depth and the pathlength distributions obeyed the exponential attenuation formula. The characteristic attenuation lengths depended on the material and electron energy. The ratio of the attenuation length for the pathlength distribution to that for the maximum depth distribution approached a value somewhat greater than two. This revealed that most electrons were backscattered from the solid through a single elastic scattering or multiple elastic scatterings.

Although experimental data on the spatial distributions are not available, we compared [9, 10] our results of Monte Carlo simulations on the reflection coefficient and the angular distribution function of elastically backscattered electrons with experimental data. The close agreement between our results and experimental data indicated the validity of present models and the accuracy of the spatial distributions of elastically backscattered electrons.

Acknowledgment

This research was supported by the National Science Council of the Republic of China under contract NSC88-2215-E-009-043.

References

[1] Kirschner J and Stab P 1973 *Phys. Lett.* **42** 335
[2] Kirschner J and Staib P 1975 *Appl. Phys.* **6** 99
[3] Gergely G 1981 *Surf. Interface Anal.* **3** 201
[4] Gergely G 1983 *Vacuum* **33** 89
[5] Gergely G 1986 *Scanning* **8** 203
[6] Mrozek P, Lesiak B and Jablonski A 1992 *Surf. Interface Anal.* **18** 403
[7] Schmid R, Gaukler K B and Seiler B 1983 *Scanning Electron Microscopy* vol 2, ed O Johari (Chicago: IIT Research Institute) p 501
[8] Jablonski A, Gryko J, Kraaer J and Tougaard S 1989 *Phys. Rev.* B **39** 61
[9] Chen Y F, Su P, Kwei C M and Tung C J 1994 *Phys. Rev.* B **50** 17 547
[10] Chen Y F, Kwei C M and Su P 1995 *J. Phys. D: Appl. Phys.* **28** 2163
[11] Kwei C M, Chen Y F and Tung C J 1998 *J. Phys. D: Appl. Phys.* **31** 36
[12] Ichimura S and Shimizu R 1981 *Surf. Sci.* **112** 386
[13] Tofterup A L 1985 *Phys. Rev.* B **32** 2808
[14] Werner W S M, Tilinin I S and Hayek M 1994 *Phys. Rev.* B **50** 4819
[15] Tung C J, Chen Y F, Kwei C M and Chou T L 1994 *Phys. Rev.* B **49** 16 684
[16] Tougaard S and Chorkendorff I 1987 *Phys. Rev.* B **35** 6570
[17] Tougaard S and Kraaer J 1991 *Phys. Rev.* B **43** 1651
[18] Borodyansky S 1992 *Surf. Interface Anal.* **19** 181
[19] Borodyansky S 1993 *Surf. Interface Anal.* **20** 811
[20] Borodyansky S and Tougaard S 1995 *Surf. Interface Anal.* **23** 689
[21] Tucker T C, Roberts L D, Nestor C W and Carson T A 1969 *Phys. Rev.* **178** 998
[22] Kwei C M, Chen Y F, Tung C J and Wang J P 1993 *Surf. Sci.* **293** 202
[23] Chen Y F and Kwei C M 1996 *Surf. Sci.* **364** 131
[24] Kwei C M, Wang C Y and Tung C J 1998 *Surf. Interface Anal.* **26** 682
[25] Reimer L 1985 *Scanning Electron Microscopy* (New York: Springer) p 114
[26] Tanuma S, Powell C J and Penn D R 1991 *Surf. Interface Anal.* **17** 911
[27] Ashley J C and Tung C J 1982 *Surf. Interface Anal.* **4** 52